

Feasibility study for mapping the polar ice bottom topography using interferometric synthetic-aperture radar techniques

**Christopher T. Allen
Manisha Gandhi
Prasad Gogineni
Ken Jezek**

**Radar Systems and Remote Sensing Laboratory
University of Kansas Center for Research, Inc.
2335 Irving Hill Road
Lawrence, Kansas 66045-7612**

**RSL Technical Report 11680-1
January 1997**

**Sponsored by:
Office of Polar Programs, National Science Foundation
Arlington, VA 22230**

Grant OPP 9523454

Section 1

Introduction

Summary

The objective of this study is to determine the system parameters for a radar echo sounding system applying interferometric synthetic-aperture radar processing for basal surface topography mapping of the thickest Greenland ice sheet. Key parameters examined include transmit power (peak and average), antenna characteristics, and signal processing algorithms, and the resultant system performance in terms of signal-to-noise ratio, subsurface scene size, and radar resolution in range, azimuth (cross-range), and height (elevation). An essential parameter in such a system-level analysis is the radar backscattering at the ice-bedrock interface, about which little information is available. Backscatter characteristics of this interface were extracted from data collected in central Greenland using the University of Kansas ICARDS radar echo sounding system [Raju, Xin and Moore (1990), Gogineni et al. (1996)].

Polar ice sheets are an integral component of the global climate system. Key elements to be determined are the mass balance, size and movement of these ice sheets. Ice bottom topography drives ice dynamics, which affects the mass balance. Accurate information of ice bottom topography will contribute to a greater understanding of the ice dynamic and improve our model of the global climate system. Essentially this topography places boundary conditions on ice flow and modifies the components of the gravitationally induced stress through local basal surface slope.

While progress has been made in radio echo sounding (RES) of ice sheets, the resultant data yield only coarse insight into the bottom topography. In traditional RES techniques, the measured range to the ice bottom is not always the range to the point directly beneath the radar—instead it is the range to the point of the closest bottom reflection to the radar. Traditional techniques of radio echo sounding of ice sheets provide valuable data on ice sheet thickness and, more recently, on internal layer structures and small-scale basal roughness [Neal, (1982)].

A few efforts to map the three-dimensional bedrock topography beneath vast ice sheets have been undertaken. As part of an experiment investigating a theoretical fifth force affecting Newton's inverse square law for gravitation, an extensive series of RES measurements were made around the DYE-3 complex in southern Greenland, where sounding data were collected along 124 radial lines, each about 5 km in length, producing a map of bedrock topography with an uncertainty of less than 5 m over most of the survey area [Fisher et al. (1989)]. More recently, a new application has emerged for the site-selection process for future deep ice core programs [Dahl-Jensen et al. (1996), Hodge et al. (1990)]. It requires finer feature resolution than

traditional radio echo sounding techniques provide. For this reason we explored the feasibility of mapping the ice bottom topography through advanced radar techniques, including synthetic-aperture radar and interferometry.

Synthetic-aperture radar (SAR) is used to produce two-dimensional maps or images of radar reflectivity for terrestrial scenes. Slant range to the target provides registration in one dimension (across-track), while the change in target echo phase with radar position (sometimes referred to as Doppler) provides position information in the other dimension (along-track). An important characteristic of SAR is that the image resolution is essentially independent of the distance between the radar and the scene. Image formation relies on a focusing process, basically a two-dimensional matched-filtering process, made possible by the a priori knowledge of the signal characteristics based on the radar-scene geometry. As SAR relies on ranging information for image reconstruction, these systems naturally require an off-nadir survey of a surface; otherwise the ranging information is unavailable.

While useful geophysical information about the scene can be extracted from a two-dimensional mapping of radar reflectivity, mapping the ice bottom reflectivity with SAR techniques has not been attempted to date. [We acknowledge the efforts of Musil and Doake (1987) and Strangway et al. (1974), though the processes applied in these efforts are not within the context of the SAR or interferometry referred to in this report.] Among the challenges to be met are contending with ice refraction, attenuation, and volume scatter effects. The required matched-filtering process requires accurate knowledge of the electrical range to a target as a function of radar position. Unknown variations in ice refraction as a function of both depth and horizontal position pose a challenge to this approach. However, SAR researchers have developed auto-focus techniques to overcome ionospheric variability for spaceborne SAR systems [Wahl et al. (1994)] that have similar characteristics to those of imaging through the glacial ice.

Through the application of interferometric SAR techniques, three-dimensional mapping of the ice bottom topography can be obtained. While SAR provides a mapping of radar reflectivity in two dimensions (range and azimuth), interferometric SAR techniques produce unambiguous three-dimensional maps of the imaged surface by comparing two, complex SAR images made from slightly different perspectives, akin to how binocular vision provides depth in human vision. We propose to determine the system characteristics required to produce an interferometric SAR image of the ice bottom topography.

Another aspect to be explored is the overall signal power requirement. As with any natural surface, the bottom surface radar backscattering characteristics (reflectivity) are greatest at nadir and, when viewed from off-nadir angles, radar backscattering decreases. This reflectivity is a function of several variables including material electrical properties, surface roughness, local slope, electrical properties of the basal ice. With few exceptions detailed information on the nature of the backscattering at the basal surface was unreported, hence we will apply proven analysis techniques, with necessary assumptions, and use existing backscattering models to provide information on this key element.

Radar frequency selection is another important consideration. Frequency determines many of the factors affecting propagation through the glacial ice, and lower frequencies generally have advantages over higher frequencies. However, other considerations such as realizable antenna characteristics and achievable image resolution will promote higher radar frequencies. A parametric evaluation of system performance is required for appropriate frequency selection.

Data collection geometry is still another consideration. Ideally airborne operation is preferred as it offers greater efficiency in large area surveys. However, ground-based data collection avoids the problem of discriminating between signals originating from the glacial top surface and those originating from the bottom surface. For airborne, off-nadir viewing angles, signals from the top and bottom surfaces can arrive back at the radar simultaneously. Compounding this problem is the fact that the signal from the top surface may be orders of magnitude larger than the signal from the bottom surface. This requires that another discriminator other than time (range) be used to separate the two signals [Doerry et al. (1994), Mader (1991)].

Section 2

Basal backscattering characteristics

Summary

Through an analysis of the ice-bedrock echo characteristics beneath the central Greenland ice sheet, physical characteristics of this basal surface are determined—specifically, the RMS height and RMS slope. Radar backscattering coefficients were then obtained using standard electromagnetic scattering models and typical values for dielectric properties of ice and bedrock. These models showed that for incidence angles greater than about 15°, the backscattering coefficient is negligible, effectively limiting the observation angle for any monostatic echo-sounding system to angles near nadir. Further, this behavior is independent of variations in system frequency within the spectrum of interest.

A key element in design and operation of a radar system is an understanding of how the target of interest will appear to the radar system. Little detailed information on the nature of the backscattering at the basal surface has been reported. Attempts to reconstruct the subglacial characteristics from RES data were reported by Harrison (1970) where he analyzed the bottom surface echo to distinguish between specular and non-specular reflections. Neal (1982) demonstrated how small-scale roughness characteristics of the basal surface could be determined from airborne RES data.

To estimate the basal surface backscattering characteristics for this study, we also applied an echo shape analysis to RES data collected by the KU ICARDS system over the central Greenland ice sheet in 1995. In this approach outlined in Elachi (1988), modeling of the interaction of the transmitted pulse as it engages the basal surface indicates how characteristics of the basal surface affect the echo rise and decay characteristics. Information gained from this analysis include the basal surface RMS height (σ_h) and the rate of change of the radar backscattering coefficient (σ^o) with respect to time (and therefore incidence angle), $d\sigma^o/d\theta$.

A modified application of this approach to our data analysis was required as the radar signal propagates through both free space (air) and the ice. As a simplifying assumption in this analysis, we ignored the fact the radar was at an altitude of 500 m above the ice surface and treated the data as if it were collected on the ice surface. The rationale behind this assumption, beyond the fact that this greatly simplified the analysis, is that the overall geometry is dominated by the thick ice sheet (thickness > 2.5 km) and the fact that the signals propagate slower in ice than air due to the refractive index of ice. Other assumptions made in this analysis include an abrupt change in refractive index at the air-ice interface (ignoring the presence of the firn layer)

and the assumption of a constant refractive index of ice for all depths, $n_{\text{ice}} = 1.78$ (while changes in density and temperature may introduce small variations with depth).

To summarize this approach, a backscattered echo from a rough surface, when illuminated by an incident pulse at normal incidence angle, will have a shape indicative of the statistical properties of the surface [Elachi (1988)]. The echo shape, $E(t)$, represents the convolution of three separate responses

$$E(t) = p(t) * S(t) * h(t), \quad (2.1)$$

where $p(t)$ is the total radar system point target response, $S(t)$ is the average flat surface response, and $h(t)$ is the observed surface elevation probability density function (PDF).

System parameters used in this analysis were characteristic of the ICARDS system and included a compressed pulse duration of 60 ns and an antenna gain pattern $G(\theta)$, with an effective antenna half-power beamwidth, θ_m , (after signal processing) of 10°

$$p(t) = \begin{cases} 1, & 0 < t < \tau \\ 0, & \text{elsewhere} \end{cases} \quad (2.2)$$

$$G(\theta) = \begin{cases} 1, & 0 < \theta < \theta_m \\ 0, & \text{elsewhere} \end{cases}. \quad (2.3)$$

The flat surface impulse response, $S(t)$, is related to the antenna gain and the surface backscattering characteristics, $\sigma^o(\theta)$, as

$$S(t) = A_o \int \delta \left[t - \frac{2 n_{\text{ice}}}{c} (r - H) \right] G^2(\theta) \sigma^o(\theta) \rho d\rho, \quad (2.4)$$

where for large values of H (height above the surface) ρ is

$$\rho = \sqrt{\left(H + \frac{c t}{2 n_{\text{ice}}} \right)^2 - H^2} \equiv \sqrt{\frac{H c t}{n_{\text{ice}}}} \quad (2.5)$$

and for $t > 0$ and the incidence angle, θ , is

$$\theta \equiv \frac{\rho}{H n_{\text{ice}}} \equiv \sqrt{\frac{c t}{H n_{\text{ice}}}}. \quad (2.6)$$

The flat surface impulse response can therefore be simplified to

$$S(t) = \begin{cases} S_o \sigma^o \left(\sqrt{\frac{c t}{H n_{\text{ice}}}} \right), & 0 < t < t_m, \\ 0, & \text{elsewhere} \end{cases} \quad (2.7)$$

where

$$t_m = \frac{H n_{ice}}{c} \theta_m^2. \quad (2.8)$$

The surface height was assumed to have a Gaussian probability distribution function (pdf)

$$h(t) = \frac{1}{\sqrt{2 \pi \sigma_h^2}} \exp\left(\frac{-c^2 t^2}{8 n_{ice}^2 \sigma_h^2}\right), \quad (2.9)$$

where σ_h is the RMS height of the surface. The backscattering coefficient was initially assumed to decrease exponentially with increasing incidence angle, characterized by a decrease of X dB for every increase in incidence angle of 10°. Finally, the ice thickness was assumed to be 2800-3000 m, corresponding to the central Greenland ice sheet thickness.

The simulated radar response was computed at time steps of 1 ns while the actual system sampled the returning echo every 53.3 ns (18.75 megasamples/s sample rate). Therefore, the simulated radar response was correspondingly resampled by keeping every 53rd sample, and ignoring the intervening 52 samples, effectively reproducing a 53-ns sample period.

Finally, the radar echo sounder is not radiometrically calibrated; i.e., absolute transmit power and system gain are not measured against a standard and are not monitored during the experiments. Therefore, only relative signal power variations are available. This is not a severe limitation, however, since signal levels can be modeled with reasonable accuracy based on well-known characteristics of the ice sheet and the radar system.

Results of this simulation were compared with several bottom echoes measured with the KU ICARDS system on May 22, 1995. Table 2.1, below, summarizes the data and simulation results.

Table 2.1. ICARDS data used in the analysis and the resulting basal surface characteristics.

Data File	Column Number	Longitude (degrees W)	Latitude (degrees N)	Ice Thickness (m)	σ_h (m)	$\Delta\sigma/\Delta\theta$ (dB/10°)	RMS slope
m22f5	902	48.1553	77.4692	2666	7	-50	0.02
m22f5	1750	47.1702	76.9846	2644	7	-50	0.02
m22f6	3601	41.7925	73.9273	3214	4	-30	0.04
m22f7	700	38.4813	72.8705	2882	7	-20	0.03
m22f7	750	39.2430	72.8602	3070	7	-30	0.03

Data from file m22f5 (May 22, fifth file) column 902 was collected at 48.1553° W, 77.4692° N, and the ice thickness measured was found to be 2666 m. This measurement is found by determining the number of pixels between the surface echo and the bottom echo, multiplying by 4.494 m/pixel, and adding 10 m (to account for the firn layer [Gundestrup, (1996)]).

Fig. 2.1 shows typical depth sounder data displayed in an A-scope format. The surface echo can be seen at around pixel number 74. Signal power prior to pixel 74 is characteristic of the depth sounder and is independent of the environment. The bottom echo can be seen at around pixel 665. Signals between pixels 74 and 665 are due to internal layering and multiple reflections (between the aircraft and the ice surface) [Allen et al. (1996)].

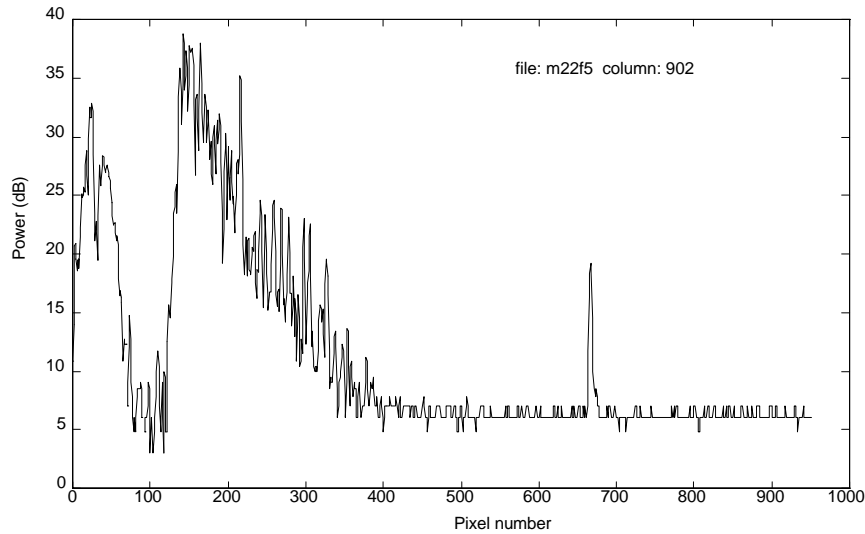


Figure 2.1. A-scope display of depth sounder data collected May 22, 1995, over the central Greenland ice sheet (position 48.1553° W, 77.4692° N).

Our analysis focused on the characteristics of the bottom echo. Fig. 2.2 shows the measured bottom echo (solid line) in a linear power scale and with an expanded time scale. Applying the technique outlined earlier, the basal surface characteristics that provide a close approximation to the measured bottom echo were found to be $\sigma_h = 7$ m and $\Delta\sigma^\circ/\Delta\theta$ of -50 dB for a change of incidence angle of 10°. For a surface with these characteristics, the predicted radar response (dashed line) will be in close agreement with the measured signal. We repeated this process on the other bottom echo data with the results summarized in Table 2.1.

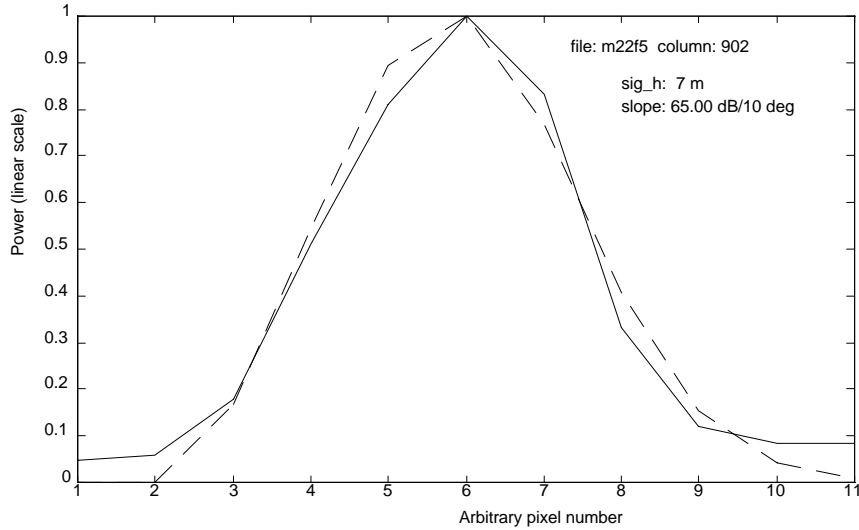


Figure 2.2. A-scope display of depth sounder data collected May 22, 1995, over the central Greenland ice sheet (position 48.1553° W, 77.4692° N). Simple exponential backscattering model. Solid line denotes measured data, dashed line denotes model fit.

Given the consistency in the basal characteristics, we next applied electromagnetic surface scattering theory to attempt to explain the observed backscattering behavior. Specifically, we found that the Kirchhoff or the Physical Optics model [Ulaby, Moore, and Fung (1982)] to be consistent with scattering from a surface with an RMS height of 4 to 7 m at this frequency (150 MHz). Again, as we were dealing with uncalibrated data (in the radiometric sense), we focused on the angular dependence. For the case of monostatic backscattering, this model simplifies to

$$\sigma_{pq}^o(\theta) = \begin{cases} \frac{|R_{pp}(0)|^2 e^{-\left(\frac{\tan^2 \theta}{2m^2}\right)}}{2m^2 \cos^4 \theta}, & \text{for } p = q, \\ 0, & \text{for } p \neq q \end{cases} \quad (2.10)$$

where $|R_{pp}(0)|^2$ is the Fresnel reflection coefficient at normal incidence (a constant), the subscripts p and q denote transmit and receive polarizations, and m^2 is the mean-squared slope of the surface; i.e., m is the RMS slope.

Using this backscattering model in the simulation, we found values for both σ_h and RMS slope for the surfaces that provided close agreement with the measured data. The results of this analysis are summarized in Table 2.1. Fig. 2.3 again shows the measured bottom echo (solid

line) along with the predicted echo based on the simulation (dashed line), now using the physical optics model to define the variation in of the backscattering coefficient with incidence angle.

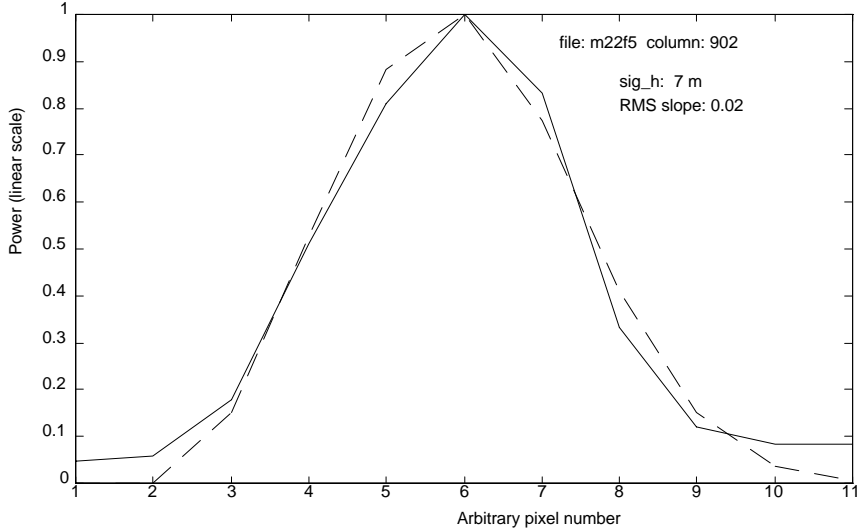


Figure 2.3. A-scope display of depth sounder data collected May 22, 1995, over the central Greenland ice sheet (position 48.1553° W, 77.4692° N). Physical optics backscattering model. Solid line denotes measured data, dashed line denotes model fit.

Based on this analysis, we developed a model for the backscattering characteristics of the bottom surface. Fig. 2.4 shows the expected backscattering coefficient (σ^o) versus incidence angle at the ice-rock interface at the basal surface for the range of RMS slopes found in the analysis. At nadir (0 incidence) the backscattering is the strongest and at angles more than 15° off nadir, the backscattering coefficient is reduced to a negligible value. This is characteristic of a nearly specular surface; however, the backscatter is purely incoherent. As a consequence, the observation angle is effectively limited for any monostatic echo sounding system to angles near nadir. Note from (2.10) that $\sigma^o(\theta)$ does not increase with frequency (reduced wavelength) so long as the prerequisite conditions are met; i.e., $\sigma_h > \lambda_{ice}$ (wavelength in ice). Therefore for σ_h of 7 m, this condition is satisfied for frequencies above 24 MHz. At significantly higher frequencies, where the small-scale surface roughness becomes a dominant backscatter contributor, there will be an increase in the backscattering characteristics and the backscattering from this surface will be dramatically different. However, at these higher frequencies the loss mechanisms within the ice will be so large (as will be seen in a later section) that this characteristic is not of interest.

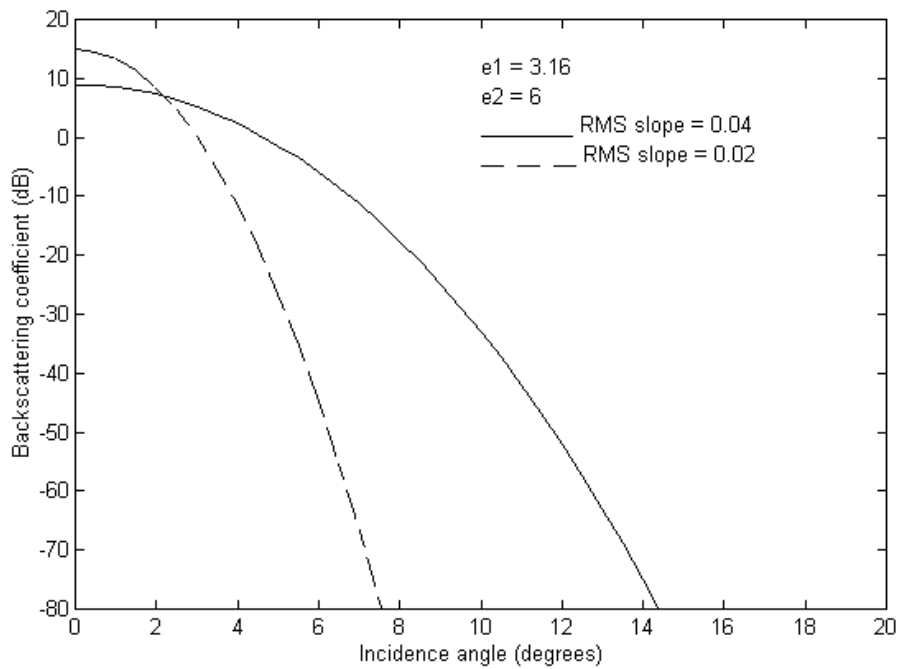


Figure 2.4. Predicted backscattering coefficient versus incidence angle based on the physical optics backscattering model with $\epsilon_1 = 3.16$ (ice) and $\epsilon_2 = 6$ (rock) and RMS slopes of 0.04 (solid line) and 0.02 (dashed line).

Section 3

Monopulse as Interferometry

Summary

The backscattering characteristics of the ice-bedrock interface beneath the central Greenland ice sheet constrained us to a nadir-looking geometry, precluding the application of traditional SAR techniques for image formation as the range extent of the scene is compressed. As an alternative, we employed Doppler beam sharpening along with monopulse radar techniques to obtain both along-track and cross-track position measurements of targets. However, to use monopulse successfully we must know the attitude of our antennas accurately, we cannot tolerate a poor signal-to-noise ratio, and must restrict our position measurements to only the highest hilltops occurring within a Doppler-beam-sharpened slice of the ice-bedrock interface.

In traditional synthetic-aperture radar (SAR), the terrain to be imaged is illuminated by the system from a nominally broadside direction permitting the processing of collected data into a two-dimensional reflectivity. Fine system resolution in the two, orthogonal dimensions, along-track and slant-range, are achieved from processing the phase history of a target (the Doppler characteristics) and from the range resolution, either from a simple, narrow pulse (brute force approach) or from a pulse compression technique. While effective departures from the broadside viewing geometry include squinting the illumination beam forward or behind the broadside direction, geometries where the target is in the plane containing the system velocity vector and the nominal surface normal of the terrain cannot employ conventional SAR, for in this region the lines of constant Doppler frequency (isodops) and the lines of constant range (isorange) are no longer orthogonal but are instead parallel. The upshot of this fact is that the two dimensions have been coalesced into a single dimension and processing does not yield a two-dimensional image.

For the application of interest in this study—that is, mapping the topography of the ice-bedrock interface beneath the central Greenland ice sheet—our choice for a monostatic radar geometry is limited to the nadir-looking case due to the backscatter characteristics of this interface (see Section 2). As a consequence of this limitation, traditional SAR techniques cannot be applied. (Note that this limitation may be unique to massive ice sheets and may not exist in other regions; e.g., beneath glaciers or ice caps.) At nadir, where the backscatter is significant, the illuminated scene falls within a few range cells so mapping of targets based on range is ineffective (see Fig. 3.1). Resolving targets in the along-track direction can still be achieved from analysis of the Doppler information in this arrangement, and, although the processes used are similar to SAR, the technique called Doppler beam sharpening [Ulaby, Moore, and Fung (1982)] is more appropriate for this application.

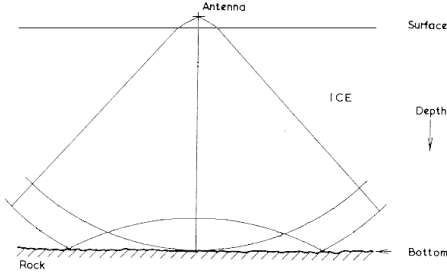


Figure 3.1. When viewed at nadir the illuminated scene falls within a few range cells, rendering the mapping of targets on the basis of range ineffective [after Robin (1975)].

In order to produce a map of the basal surface topography, a means of measuring the cross-track target position is required, and for this we propose to apply a monopulse technique. Monopulse systems use specialized antenna configurations that output two or more radio frequency signals that, through appropriate signal processing, determine the target angle relative to the antenna boresight. Briefly, the scene of interest is illuminated from one or more antennas and the backscattered signal is received by two (or more) antenna apertures. Depending on the design of the system, the signals received by the two antennas (v_1 and v_2) will differ either in amplitude or phase (or both), and this difference is used to determine the angle off-axis. In one-axis monopulse systems, a single angle is output while in two-axis systems, two orthogonal angles are output. We propose applying the monopulse approach by having two identical antennas mounted along an axis perpendicular to the velocity vector of the system in order to measure the cross-track angle of the target. Each antenna output would drive a separate receiver channel, followed by a digitizer. The data would then be processed digitally to obtain the off-axis angle using

$$\theta = \frac{1}{k_m} \frac{d}{s}, \quad (3.1)$$

where θ is the off-axis angle, k_m is the slope of the monopulse response curve versus the off-axis angle, and d/s is the normalized difference signal derived from the two channels (the difference signal $d = v_1 - v_2$, and the sum signal $s = v_1 + v_2$).

It should be noted that this scheme has been successfully applied in the past at Sandia National Laboratories [Callahan et al. (1986)] for obtaining position information from local topography using a nadir-looking, aircraft-based altimeter. In addition, this scheme is being proposed [Jensen, and Raney (1996)] for a space-based altimeter for continental ice-sheet measurement.

While this approach provides information essential for this application, it brings with it some limitations. Specifically, for accurate angle measurements, three conditions must be met: (i) the attitude (roll angle) of the antennas must be known to the desired accuracy, (ii) the accuracy this approach will not provide accurate angle estimates for unresolved targets, and (iii) the signal-to-noise ratio of the data is a factor determining the magnitude of the angle error. Both the first and second conditions affect implementation. Regarding the first condition, without going into detail, this approach has been implemented previously using 1980s technology, from which it is evident that the means exist to determine the antenna attitude accurately.

The prohibition on unresolved targets tells us that in order to estimate the angle accurately the target must be a point target; i.e., one that appears to the radar to be concentrated at a point in angle space [Sherman (1984)]. From an operational viewpoint, this prevents us from determining the off-axis angle of every scatterer at the basal surface interface and instead tells us that we can only determine the cross-track angle for portions of the interface that can appear isolated. What this means is that we can only measure the angle to the highest hilltops that occur within a Doppler-beam-sharpened slice of the terrain and only if we can resolve the signal from this portion of the terrain from the rest of the terrain; i.e., if the height difference is greater than the radar's range resolution. The system's range resolution requirements must be selected appropriately depending on the anticipated surface relief at this interface. Given the analysis in Section 2, where we saw an RMS height of around 7 m for a region where the interface is nominally flat, if we desire to map elevation variations on this level, we would require a system range resolution to be much less than this, approximately 0.5 to 1 m. If, on the other hand, we desire to map the coordinates of *significant* features (i.e., hilltops well above the local terrain), then a coarser range resolution would be adequate.

The third condition, which relates the signal-to-noise ratio (SNR) to angle error, clearly impacts the radar system design. Sherman (1984) tells us that the standard deviation of the angle error, σ_θ , is related to the SNR, the beamwidth of the antenna pattern, θ_{bw} , and the number of pulses whose measurements are averaged to obtain the angle estimate by

$$\sigma_\theta = \frac{\theta_{bw}}{k_m \sqrt{2 n S/N}} \left[1 + \left(\frac{d}{s} \right)^2 \right]^{\frac{1}{2}}. \quad (3.2)$$

As a point of reference, Callahan et al. (1986) set as a minimum an SNR of about 20 (13 dB) for their system.

Section 4

Signal Propagation and Power

Summary

The peak transmitter power necessary to provide an adequate signal-to-noise ratio was evaluated through the application of the radar equation adapted for the desired geometry, using baseline radar parameters from the ICARDS radar. Signal attenuation through the ice was estimated based on reported loss tangent values for ice and proposed scattering losses. The results indicated that the required peak transmitter power depends on whether the scattering loss is significant; however, insufficient data are available to clarify this issue. Monopulse cross-track resolution improves for high frequencies due to the fixed antenna size assumed.

Signal Power

The received signal-to-noise ratio depends on several factors, which are represented in the radar equation for the geometry shown in Fig. 4.1, [Mader (1991), Chuah (1996)]

$$P_t = \frac{\text{SNR} (4\pi)^3 R_{QB}^2 R_{OT}^2 k T_o F B_{RX}}{T B_{TX} \sigma^o A G^2 \lambda^2 e^{-4\alpha R_{PB}} (1 - |R_{ia}|^2) (1 - |R_{ai}|^2) N_{coh} \sqrt{N_{incoh}}}, \quad (4.1)$$

where

P_t is the transmitted power (peak);

SNR is the signal-to-noise ratio in the receiver;

R_{QB} , R_{OT} , and R_{PB} are the ranges shown in Fig. 4.1;

k is Boltzmann's constant (1.38×10^{-23} J/K);

T_o is the physical temperature of the receiver;

F is the noise figure of the receiver;

B_{RX} is the receiver bandwidth;

T is the pulse duration of the transmitted signal;

B_{TX} is the bandwidth of the transmitted signal;

σ^o is the backscattering coefficient of the ice-bedrock surface;

A is the area illuminated by the antenna;

G is the antenna gain;

λ is the signal wavelength in free space;

α is the attenuation constant;

R_{ia} and R_{ai} are the reflection coefficients the air/ice and ice/air boundaries;

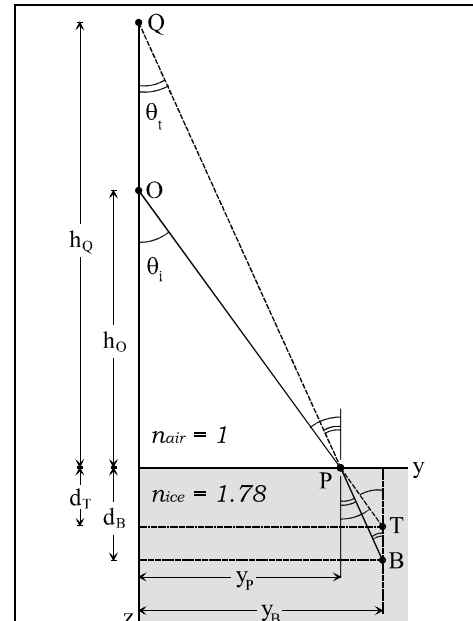


Figure 4.1 Geometry of radar sounding through a homogeneous dielectric [after Mader (1991)].

N_{coh} is the number of coherent integrations; and

N_{incoh} is the number of incoherent integrations.

Note that for nadir-looking geometries R_{PB} is the ice thickness and $R_{QB} = R_{OT}$.

To determine the required signal power for specific system parameters, (4.1) will be evaluated requiring that non-system parameters (σ^o , R_{ia} , R_{ai} , α) be determined. The issue of the backscattering characteristics at the ice-bedrock surface has already been addressed in Section 2.

Reflections Coefficients at the Air-Ice Boundary, R_{ia} and R_{ai}

Assuming a planar interface at the air-ice boundary, and again assuming an abrupt transition between air and ice (i.e., no firn layer), we can determine conservative estimates for R_{ia} and R_{ai} from

$$R_{ai,V} = \frac{\cos\theta_{ice} - n_{ice} \cos\theta_{air}}{\cos\theta_{ice} + n_{ice} \cos\theta_{air}} = -R_{ia,V} \quad (4.2a)$$

$$R_{ai,H} = \frac{\cos\theta_{air} - n_{ice} \cos\theta_{ice}}{\cos\theta_{air} + n_{ice} \cos\theta_{ice}} = -R_{ia,H}, \quad (4.2b)$$

where the subscripts V and H denote vertical and horizontal polarizations and θ_{air} and θ_{ice} refer to the angle between the signal Poynting vector and the surface normal and are related through Snell's law. As we are constrained to near normal angles (due to the backscattering characteristics), θ_{air} and θ_{ice} will both be so small that the cosine of these small angles can be approximated as unity, removing the polarization dependence and simplifying these expressions to

$$R_{ai} \equiv -R_{ia} \equiv \frac{1 - n_{ice}}{1 + n_{ice}} = 0.28 \quad (4.3)$$

or $|R_{ia}|^2 = |R_{ai}|^2 = 0.079$ or -11 dB.

Attenuation Constant, α

For a low-loss medium, such as ice, the attenuation constant, α , due to dielectric absorption can be expressed as

$$\alpha = \frac{k_{ice} \tan \delta}{2}, \quad (4.4)$$

where the loss tangent, $\tan \delta$, represents the ratio of the imaginary part to the real part of the relative permittivity of the medium (ice),

$$\tan \delta = \frac{\sigma}{\omega \epsilon} = \frac{\epsilon''_{\text{ice}}}{\epsilon'_{\text{ice}}} , \quad (4.5)$$

and k_{ice} is the wave number in the medium (ice)

$$k_{\text{ice}} = \frac{2\pi f}{c} n_{\text{ice}} . \quad (4.6)$$

Here f is the signal frequency (Hz), c is the free-space speed of light (m/s), and n_{ice} is the refractive index of ice, which is related to the real part of the relative permittivity by

$$n_{\text{ice}} = \sqrt{\epsilon'_{\text{ice}}} . \quad (4.7)$$

Hence, the expression for the attenuation constant can be simplified as

$$\alpha = \frac{\pi f}{n_{\text{ice}} c} \epsilon''_{\text{ice}} . \quad (4.8)$$

Experimental evidence indicates that for fresh-water and pure-water ice, the real part of the relative permittivity may be considered independent of both temperature (below 0° C) and frequency in the microwave region and may therefore be assigned a constant value, $\epsilon' = 3.15$ [Ulaby, Moore, and Fung (1986)]. This value has been confirmed experimentally by relating the observed ice thickness at a site where the ice thickness is known (from a bore hole) and determining a corresponding value for n_{ice} .

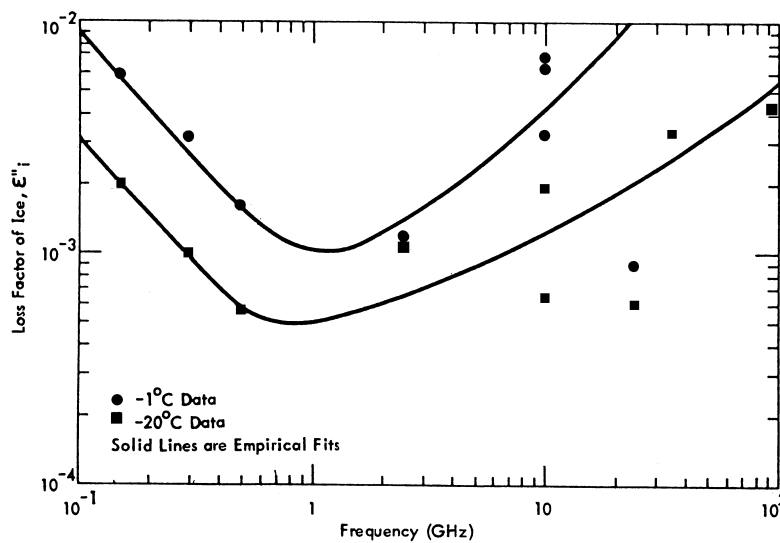


Figure 4.2. Loss factor of pure- and fresh-water ice [after Ulaby, Moore, and Fung (1986)].

The imaginary part of the relative permittivity, ϵ'' , depends on frequency and temperature [Ulaby, Moore, and Fung (1986)] as shown in Fig. 4.2. We empirically fit an expression to the measured data to obtain

$$\epsilon'' = \frac{1}{10f} 10^{-2.02 + 0.025T}, \quad (4.9)$$

where T is the physical ice temperature in $^{\circ}\text{C}$ (always a negative value) and f is the frequency expressed in GHz. Strictly speaking, this relationship is only valid for frequencies from 100 MHz to about 700 MHz and temperatures from -1° C and -20° C . Clearly, from Fig. 4.2 it can be seen that trend toward smaller values of ϵ'' changes to a trend of increasing values with increasing frequency at a frequency of around 800 to 1000 MHz. Due to the limited quantity of data and the large variation within the available data, a more accurate estimation of this parameter is not possible. We will constrain our use of this model to the frequencies indicated; however, we will extend its application to ice temperatures of -30° C to model loss in ice near the Greenland summit.

Combining (4.8) and (4.9) we get

$$\alpha = \frac{0.955 \times 10^6 \pi}{n_{\text{ice}} c} 10^{0.025T}, \quad (4.10)$$

which is independent of frequency (up to around 700 MHz).

We know that ice temperature depends on depth as well as distance from the ice-sheet center, and Fig. 4.3 shows estimated temperature distribution across central Greenland [Robin (1972)].

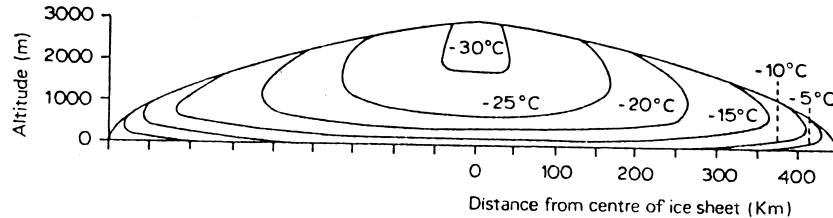


Figure 4.3. Cross section of temperature distribution across central Greenland [after Robin (1972)].

Using the temperature distribution shown, we fit an expression for the ice temperature as a function of height above the bottom as

$$T_{\text{ice}} = -30 + 20 e^{-\frac{z}{750}}, \quad (4.11)$$

where T_{ice} is in $^{\circ}\text{C}$ and z is in meters. Using this relationship for a nadir-looking system at the summit (thickness of 3000 m), we found an overall value for α of 1.4×10^{-3} Neper/m and a total two-way attenuation due to absorption through 3 km of ice of about 73 dB. For comparison, from an analysis of the ICARDS system data we estimate a total attenuation of about 80 dB for the thickest ice [Chuah (1996)].

The remaining 7 dB of signal attenuation may be attributed to scattering loss or other unaccounted-for phenomena. Scattering from such sources as air bubbles and dust particles, which will have different spatial distributions [The Amanda Collaboration (1995)], are both much smaller than the signal wavelength. Therefore Rayleigh scattering is expected, and the related loss will increase with increasing frequency as f^4 . This scattering loss mechanism, if significant at 150 MHz (ICARDS frequency), will be 4.7 times greater in frequency at 700 MHz , increasing by a factor of 488 or 27 dB.

Required Transmit Power

To evaluate the peak transmitter power to provide a 13-dB SNR, system parameters were assumed as listed in Table 4.1 below. Many of these values are characteristics from the ICARDS radar, which is serving as a baseline. A constant antenna size was assumed, resulting in an antenna gain that is frequency dependent as

$$G = \frac{4\pi A_L A_w \eta}{\lambda^2}, \quad (4.12)$$

where A_L and A_w represent the effective length and width of the antenna, respectively, and η is the antenna efficiency. In fact, an effective gain increase may result from signal refraction due to a focusing of the downwelling signal—this slight gain, which would be frequency independent, has been ignored in these calculations.

The target area (A) of 25,000 m^2 was selected to represent a square cell approximately 160 m x 160 m, where 160 m is the along-track resolution of the ICARDS system, assuming a comparable resolution in the across-track direction.

Table 4.1 Nominal radar parameters used to evaluate required peak transmitter power

Parameter	Value	Units
SNR	20	dB
Aircraft altitude (above ice surface)	500	m
T _o	290	K
F	2.5	
B _{RX}	20	MHz
T	1.6	μs
B _{TX}	17	MHz
N _{coh}	256	samples
N _{incoh}	4	samples
A _L	1	m
A _w	3	m
η	0.6	
A	25000	m ²

Given these assumptions, the required peak transmitter power was determined using (4.1) for radar frequencies from 60 MHz to 700 MHz, and the results are shown in Fig. 4.4. Note that despite the fact that the loss due to absorption is frequency independent in this frequency range, the required transmitter power increases, due to the assumed Rayleigh scattering loss that increases at a f^4 rate. If the scattering loss is insignificant (the residual loss is frequency independent), then the required peak transmitter power decreases with increasing frequency as shown in Fig. 4.5. Unfortunately, insufficient data are available to resolve this uncertainty.

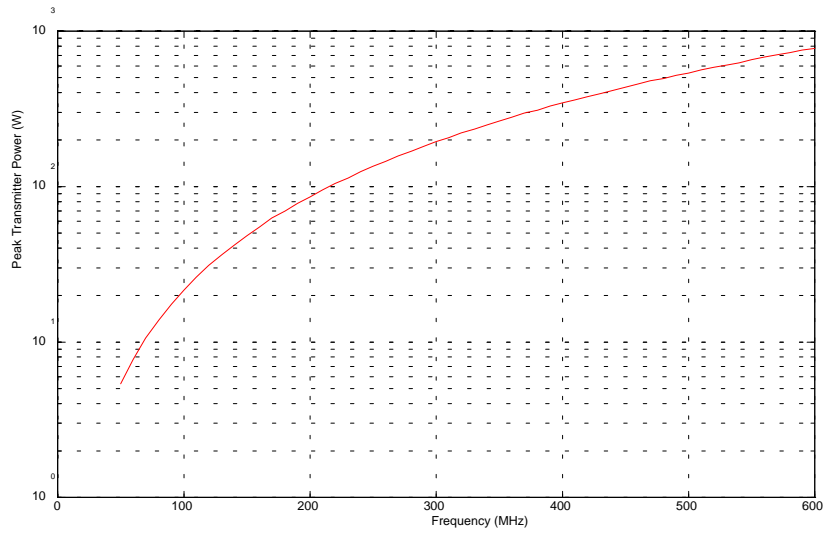


Figure 4.4. Required peak transmitter power as a function of system operating frequency for the case of significant Rayleigh scattering loss in the ice.

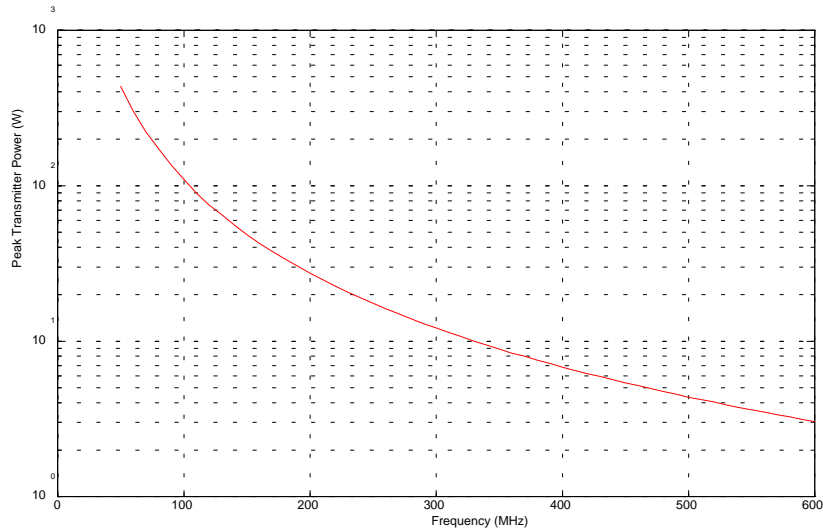


Figure 4.5. Required peak transmitter power as a function of system operating frequency for the case where Rayleigh scattering loss in the ice is not significant.

Angular Resolution

For the scenario examined above with a fixed antenna aperture, the resultant antenna beamwidth will decrease with increasing frequency and a corresponding decrease (improvement) in cross-track resolution is obtained. If the monopulse process improves angular resolution by a factor of ten (a reasonable capability), then the cross-track resolution would be related to the antenna beamwidth in the cross-track direction, or

$$\theta_x = \frac{\beta_x}{10} = \frac{\lambda}{10 A_w}. \quad (4.13)$$

The corresponding cross-track resolution for the scenario examined above is shown in Fig. 4.6 and clearly improves with increasing frequency.

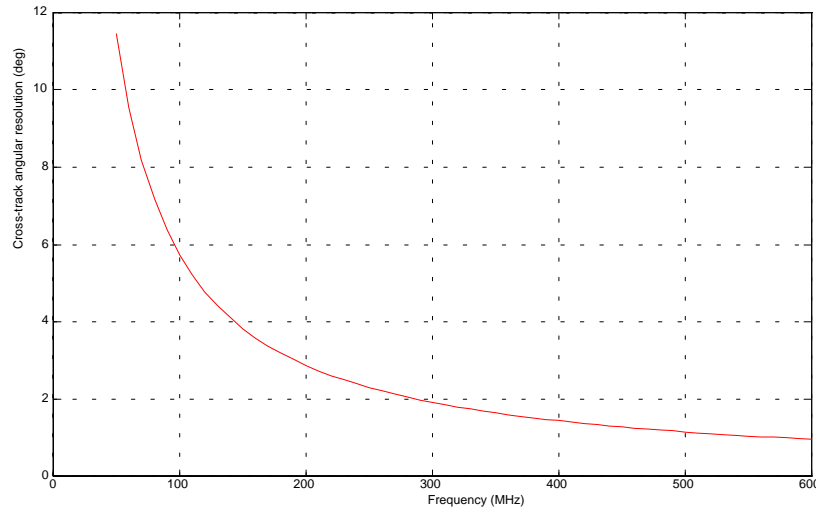


Figure 4.6. Cross-track resolution as a function of system operating frequency for a fixed antenna aperture size.

Section 5

Conclusions

Topography of the basal surface is a significant factor in ice dynamics, which is an important component of a global climate model. At radio frequencies, the ice sheet has a sufficiently low loss to permit observation of the ice-bedrock interface and radio echo-sounding (RES) has been used for many years to measure ice thickness. Application of advanced radar techniques such as synthetic-aperture radar and interferometry, which require specific data collection geometries relative to radar motion to provide topographic mapping, cannot be applied due to near-specular backscattering characteristics of this interface, at least for regions beneath the central Greenland ice sheet. As an alternative, a means of providing some topographic information for this interface is proposed employing Doppler beam sharpening and monopulse angle measurement from a nadir-looking radar. Monopulse is useful here only for the case where only one localized scatterer is within the resolved cell (constrained in the range and along-track directions). As a consequence, we will be able to map the position of the local terrain peaks to a high degree of precision within the basal surface topography.

We examined the required system characteristics for this arrangement and found them to be comparable in magnitude to modern RES systems (e.g., the ICARDS system). An unresolved question regarding losses due to scattering has the potential to impact significantly the required transmitter signal power at higher operating frequencies, where monopulse techniques provide improved cross-track resolution.

For further study, examination of the basal scattering characteristics beneath ice masses other than the central Greenland ice sheet would reveal whether the conclusions drawn from this study pertain to these other regions as well.

References

- Allen, C.T., S. Gogineni, B. Wohletz, K. Jezek, and T.S. Chuah, "Airborne radio echo sounding of outlet glaciers in Greenland," submitted to *International Journal Remote Sensing Letters*, 1996.
- The Amanda Collaboration, "On the age vs. depth and optical clarity of deep ice at the South Pole," *Journal of Glaciology*, 41(139) pp. 445-454, 1995.
- Callahan, M. et al., "Directional altimeter documentation," Sandia National Laboratories, unpublished, 1986.
- Chuah, T.S., "Design and development of a coherent radar depth sounder for measurement of Greenland ice sheet thickness," University of Kansas Department of Electrical Engineering and Computer Sciences D.E. Dissertation, p. 26, December 1996.
- Dahl-Jensen, D., N.S. Gundestrup, K.R. Keller, S.J. Johnsen, S.P. Gogineni, C.T. Allen, T.S. Chuah, H. Miller, S. Kipstuhl, and E.D. Waddington, "A search in North Greenland for a drill site," submitted to *Journal of Glaciology*, 1996.
- Doerry, A.W., B.C. Brock, B. Boverie, and D. Cress, "Imaging targets embedded in a lossy half space with synthetic aperture radar," *Proceedings of the 1994 International Geoscience and Remote Sensing Symposium*, Pasadena, California, pp. 2508-2512, Aug. 1994.
- Elachi, C., *Spaceborne Radar Remote Sensing: Applications and Techniques*, IEEE Press, New York, New York, pp. 187-190, 1988.
- Fisher, E., G. A. McMechan, M. R. Gorman, A. Paul, R. Cooper, C. L. V. Aiken, M. E. Ander, and M. A. Zumberge, "Determination of bedrock topography beneath the Greenland ice sheet by three-dimensional imaging of radar sounding data," *Journal of Geophysical Research*, 94(B3) pp. 2874-2882, 1989.
- Gogineni, S.P., T.S. Chuah, K.C. Jezek, C.T. Allen, and R.K. Moore, "An improved coherent radar depth sounder," in preparation, University of Kansas, 1996.
- Gundestrup, N., personal communication, 1996.
- Harrison, C. H., "Reconstruction of subglacial relief from radio echo sounding records," *Geophysics*, 35(6), pp. 1099-1115, 1970.

Hodge, S.M., D.L. Wright, J.A. Bradley, R.W. Jacobel, N. Skou, and B. Vaughn, "Determination of the surface and bed topography in Central Greenland," *Journal of Glaciology*, 36(122), pp. 17-30, 1990.

Jensen, J.R., and R.K. Raney, "Multi-mission radar altimeter: concept and performance," *Proceedings of the 1996 International Geoscience and Remote Sensing Symposium*, Lincoln, Nebraska, pp. 2279-2281, May 1996.

Mader, R.E., "Synthetic-aperture radar imaging of glacial ice," University of Kansas Department of Electrical and Computer Engineering Master's Thesis, October 1991.

Musil, G. J., and C. S. M. Doake, "Imaging subglacial topography by synthetic aperture radar technique," *Annals of Glaciology*, 9, pp. 170-175, 1987.

Neal, C. S., "Radio echo determination of basal roughness characteristics on the Ross ice shelf," *Annals of Glaciology*, 3, pp. 216-221, 1982.

Oswald, G. K. A., "Investigation of sub-ice bedrock characteristics by radio-echo sounding," *Journal of Glaciology*, 15(73), pp. 75-87, 1975.

Raju, G., W. Xin, and R. K. Moore, "Design, development, field observations, and preliminary results of the Coherent Antarctic Radar Depth Sounder (CARDS) of the University of Kansas, U.S.A.," *Journal of Glaciology*, 36(123), pp. 247-254, 1990.

Robin, G. de Q., "Polar ice sheets: a review," *The Polar Record*, 16(100), pp. 5-22, 1972.

Robin, G. de Q., "Radio-echo sounding: glaciological interpretations and applications," *Journal of Glaciology*, 15(73), pp. 49-64, 1975.

Sherman, S.M., *Monopulse Principles and Techniques*, Artech House, Norwood Massachusetts, p. 298, 1984.

Strangway, D. W., G. Simmons, G. LaTottaca, R. Watts, L. Bannister, R. Baker, J. D. Redman, and J. R. Rossiter, "Radio-frequency interferometry—a new technique for studying glaciers," *Journal of Glaciology*, 13(67) pp. 123-132, 1974.

Ulaby, F.T., R.K. Moore, and A.K. Fung, *Microwave Remote Sensing*, Vol. II, Artech House, Norwood, Massachusetts, pp. 925-936, 1982.

Ulaby, F.T., R.K. Moore, and A.K. Fung, *Microwave Remote Sensing*, Vol. III, Artech House, Norwood, Massachusetts, pp. 2026-2028, 1986.

Wahl, D. E., P. H. Eichel, D. C. Ghiglia, and C. V. Jakowatz, Jr., "Phase gradient auto-focus—a robust tool for high resolution SAR phase correction," *IEEE Transactions on Aerospace and Electronic Systems*, 30(3), pp. 827-835, July 1994.